C.P. No. 514
(19,868)
A.R.C. Technical Report

C.P. No. 514
(19,868)
A.R.C. Technical Report

MINISTRY OF AVIATION

AERONAUTICAL RESEARCH COUNCIL

CURRENT PAPERS

Wind Tunnel Measurements of Lift, Drag and Pitching Moment of Two Highly Swept (Λ_{LE}=87 deg. and 81 deg.) Delta Wing-Body Combination Models with Small Tip Fins at M=2·47

by

P. J. Bateman

LONDON: HER MAJESTY'S STATIONERY OFFICE

1960

FOUR SHILLINGS NET

C.P. No.514

U.D.C. No. 533.691.13.043.2:533.6.011.5:

Technical Note No. Aero 2449

May, 1957

ROYAL AIRCRAFT ESTABLISHMENT

Wind Tunnel Measurements of Lift, Drag and Pitching Moment of two highly swept (Λ_{LE} = 87° and 81°) delta wing-body combination models with small tip fins at M = 2.47

by

P.J. Bateman

SUMMARY

Tests have been made to explore the aerodynamic possibility of a feasible aircraft design based on a highly swept (over 80°) delta planform with sufficient body depth in the region of the centre of gravity to accommodate the lifting jet engines required for take-off and landing. Two models were tested, of 87° and 81° leading edge sweepback respectively.

The initial lift curve slope is greater than slender body theory would predict for the wing-body combination due partly to the presence of tip fins, and the subsequent non-linearity is greater for the more highly swept model. Drag measurements agree with estimates reasonably well and full scale lift/drag ratios of 4.2 for the 87° configuration and 5.8 for the 81° configuration are indicated on the basis of the tunnel results.

The pitching moment coefficient measured about the mean quarter-chord point is shown to vary fairly linearly with C_L for the 81° model, but the aerodynamic centre tends to move forward slightly (i.e. destabilising) with increasing incidence for the 87° model.

LIST OF CONTENTS

		Page
1	Introduction	4
2	Models	4
3	Extent of Tests	4
4	Accuracy	5
5	Results and Discussion	5
	5.1 Lift	5
	5.11 Lift 87° Model	5
	5.12 Lift 81° Model	6
	5.2 Drag	7
	5.21 Zero Lift Drag	7
	5.22 Drag due to Lift	8
	5.3 Lift/Drag Ratio	9
	5.4 Pitching Moment and Centre of Pressure Position	9
	5.5 Flow Visualisation	10
6	Conclusions	10
References		11

LIST OF ILLUSTRATIONS

	Figure
Leading dimensions of 87° Model	1
Leading dimensions of 81° Model	2
C_L vs. α for both Models at M = 2.47	3
Effect of tip fins on initial lift curve slope for 87° Model	4
C_D vs. C_L for both Models at M = 2.47	5
ΔC_x and $-C_z\alpha$ vs. $-C_z$ for 81° Model at M = 2.47	6
L/D vs. C_L for both Models at M = 2.47	7
C_m vs. C_L for both Models at M = 2.47	8
C.P. vs. α for both Models at M = 2.47	9
Flow pattern on upper surface of 81° Model at M = 2.47 (diagrammatic)	10
Flow pattern on upper surface of 81° Model at M = 2.47	11

LIST OF SYMBOLS

A	aspect ratio = span^2 ÷ planform area
$\bar{\bar{c}}$	mean aerodynamic chord
C_D	drag ÷ $\frac{1}{2}\rho U^2 S$ ($\equiv -C_X \cos\alpha - C_Z \sin\alpha$)
C_{D_O}	zero-lift drag coefficient
C_{D_F}	friction drag coefficient
C_{D_W}	wave drag coefficient
C_L	lift ÷ $\frac{1}{2}\rho U^2 S$ ($\equiv C_X \sin\alpha - C_Z \cos\alpha$)
$C_{L\ opt}$	lift coefficient for maximum L/D
C_m	pitching moment ÷ $\frac{1}{2}\rho U^2 S\bar{\bar{c}}$
C_X	axial force ÷ $\frac{1}{2}\rho U^2 S$
ΔC_X	increment of axial force with incidence
C_Z	normal force ÷ $\frac{1}{2}\rho U^2 S$
D	drag
ℓ	nominal body length (= 9 in.)
L	lift
M	pitching moment; also free stream Mach No.
Re	Reynolds number
S	planform area
S_c	maximum cross-sectional area
U	free stream velocity
x,y,z	orthogonal, right handed body axes, with the x-axis forward facing along the principal longitudinal body axis, the y-axis to starboard in the plane of the wings, and the z-axis perpendicularly downwards. The origin is $4\frac{1}{2}$" aft of the model nose
X,Y,Z	components of force along the x,y, and z axes respectively
α	angle of incidence
ε	apex semi-angle of delta planform
ρ	free stream air density

1 Introduction

Interest has arisen in the highly swept delta planform on account of its possible low drag and small change of aerodynamic centre with speed, but due to the low lift available at landing and take-off speeds with such a planform auxiliary lifting machinery would appear necessary. The inclusion of a merged body of revolution in the models tested represents an attempt at providing a closer approximation to a feasible aircraft by providing sufficient body depth in the region of the centre of gravity to accommodate lifting engines. This note gives results of wind tunnel measurements made at $M = 2.47$ of normal force N, axial force A, and pitching moment M on two highly swept delta wing body combination models, expressed for convenience as lift, drag and pitching moment.

2 Models

The models tested were manufactured in steel from the solid, and are optimum bodies of revolution for given length and frontal area* of 6% fineness ratio faired into delta wings of RAE 101 section 6% thick with leading edges tangential to the body profile (see Figs. 1 and 2). The models are symmetrical top and bottom and have leading edge sweepback angles of 87° and 81° respectively. The intersection of the leading and trailing edges produced occurs at the same longitudinal station in both models and this determines the trailing edge sweepforward angle. This leads to the planform of the 81° model being determined by the wings entirely but in the case of the 87° model the wing is faired into the body planform at a station some 24% of the centreline chord from the nose. Thus the most forward sections of this model are circular and evolve into body-wing type sections further aft. The principal dimensions of these models are given in Figs. 1 and 2.

Flat plate type wing tip fins with chamfered leading edges are incorporated simulating the laterally projected area of the minimum-size engine nacelles required to provide the thrust, but considerations of lateral stability are expected to require these to be increased.

3 Extent of Tests

The tests were carried out in the No. 6 11" × 6", supersonic wind tunnel at R.A.E. The Mach number of the tests was 2.47 and the stagnation pressures used were 1 and 2.3 atmospheres giving Reynolds numbers of $2\frac{1}{4}$ and $5\frac{1}{4} \times 10^6$ respectively based on centreline chord. A three component strain gauge balance was used with self-balancing bridges to measure normal force, axial force and pitching moment, which were converted to lift, drag and pitching moment for presentation.

In addition acenaphthalene and azo-benzine indicating coatings, and titanium oxide films were used to obtain a picture of the boundary layer flow conditions. Tests were repeated with transition forced by a 0.006"

---

*The equation of these bodies was developed by Lighthill[1] and is given by:-

$$\frac{r}{\ell} = 0.03 \sqrt{(1 - \xi^2)^{\frac{1}{2}} - \xi^2 \operatorname{sech}^{-1} |\xi|}$$

where $\xi = \frac{2x}{\ell}$

ring around the body 1.55" aft of the nose in the case of the 87° model, and by a 0.006" diameter wire behind the leading edge of the 81° model.

Each model was traversed in incidence by intervals of half a degree over a range permitted by the sting deflection inside a fixed wind shield, and at the higher stagnation pressures this range was just sufficient to cover the $C_{L\ opt}$ for maximum L/D. This limitation was imposed in the interests of maximum sting sensitivity and minimum base correction error.

Different normal force and pitching moment sting balances were used for each model but the axial force balance used was common to both and consequently resulted in a lower standard of accuracy for the 87° model particularly at the lower stagnation pressure.

Calibration of the balances was by changing weights to simulate normal force, varying the position to obtain moment changes, and weights acting over a pulley were used to provide axial force. Simultaneously, model angular deflection in incidence plane with load was measured by means of dial test indicators. A calibration correction was applied for temperature effect which in practice is kept as small as possible by controlling stagnation temperature.

4 Accuracy

In assessing the accuracy of these tests the following sources of error have been considered.

(1) Calibration scatter.

(2) Reading resolution of scales.

(3) Hysteresis in temperature calibration.

(4) Accuracy of setting incidence gear.

Experimental technique was arranged to minimise the effects of all of these sources of errors and in fact, the test results suggest that the estimated accuracy given below is pessimistic.

Table I

Re ÷ 10^6	87° Model		81° Model	
	$2\frac{1}{4}$	$5\frac{1}{4}$	$2\frac{1}{4}$	$5\frac{1}{4}$
C_L	±0.0025	±0.0041	±0.0019	±0.0009
C_m	±0.0008	±0.0004	±0.0028	±0.0014
C_{D_0}	±0.0005	±0.0002	±0.0002	±0.0001
C_D	±0.0008	±0.0004	±0.0005	±0.0003
α°	±0.05	±0.05	±0.05	±0.05

5 Results and Discussion

5.1 Lift

5.11 Lift on 87° Model

The measured values of C_L against α for the more slender model are plotted in Fig. 3, points being recorded at two stagnation pressures both with

and without a transition ring around the nose. The experimental values show that slightly higher lift was obtained at the higher Reynolds number, but not sufficiently so to warrant drawing two lines through the points. The transition ring apparently had no effect on the lift.

The "cross-sectional aspect ratio"* of this model is smaller than for the 81° model, being a body of revolution for the first quarter of its length, and it may be seen from Fig. 3 that the lift curve is more non-linear than that of the 81° model. The slope of the initial linear part of the lift curve was measured as 0.4 to 0.45, but it extended no further than three degrees of incidence.

The measured value of the lift curve slope at both Reynolds numbers is considerably in excess of slender body theory. A subsequent measurement with fins removed has indicated that the fin-wing interaction is only partially responsible for this higher lift.

Some unpublished results of lift measurements on an 87° model at low subsonic speeds with several sizes of tip fin are shown in Fig. 4. The present wind tunnel test results with and without fins are also included together with one approximate value for a free flight version of the same model, but with larger fins, and flying at speeds between M = 1.8 and 1.3. From this figure it is seen that the initial lift curve slopes at supersonic speeds are somewhat greater than for the corresponding configuration at low speeds.

The non-linearity increases with incidence rising from α to the power 1.0 at 3° incidence to α to the power 1.8 at 9°, staying constant thereafter over the range tested. Estimates based on the method of Küchemann[2] which gives $C_L = \frac{\pi A}{2}\alpha + \frac{\pi^2}{4} A\alpha^{\frac{3}{2}}$, underestimate the non-linearity in the upper incidence range.

5.12 Lift on 81° Model

The lift curve for this model also is given in Fig. 3. Points are shown for the two Reynolds numbers and for tests with and without transition fixed by a wire on the upper surface. The effect of these variations is not sufficiently large for any clear distinctions to be made; accordingly, a single curve has been drawn through all points.

The variation of lift appears to be linear to an incidence of 4° or 5°, and to increase non-linearly from this incidence onwards. This has been observed previously for example in ref. 3. The slope of the initial linear portion is approximately 0.95 per rad and is again considerably in excess of that predicted by slender body theory for a planform of the same aspect ratio without tip fins. The non-linear increment in slope is less than that predicted by Küchemann in ref 2 for a simple delta with sharp leading edges and of the same aspect ratio.

Also in Fig. 3 shown for comparison are curves based on Küchemann's equation and the slender body slope of 0.75. It should be noted that although Küchemann's analytical curve disregarding tip effect appears to yield a close approximation to the measured points the zero lift curve slope, i.e. the slender body figure of 0.75, is considerably lower than that measured viz 0.95-1.00.

---

*i.e. The ratio of the square of the local span to the cross-sectional area.

5.2 Drag

Drag curves are presented in Fig. 5. The true axial-force is obtained from the balance axial-force measurement, together with a tare correction due to the gravitational term as incidence is varied, and a correction of the base pressure as measured in the drag unit shroud, to the calculated free stream static pressure. The accuracy required for deducing whether there is a forward component of axial-force due to incidence, i.e. whether there is any effective leading edge suction, is probably beyond the capabilities of the balance until incidences of some 6° or 7° are reached in the case of the 87° model. In the case of both models however it is sufficient at $C_{L\ opt.}$ to make a useful estimate of the proportion of effective leading edge suction realised.

5.21 Zero Lift Drag

Estimates of drag due to friction have been made for both models based on a strip theory of local Reynolds number for fully laminar and fully turbulent flow. The assumption made was that the mean friction coefficient was a linear function of the percentage of turbulent flow area present as deduced from boundary layer indicator tests. The estimates of wave drag were based on simple area rule worked out for smoothed versions of both models, giving wave drags independent of Mach number. The results, evaluated numerically from the ordinates of the area distribution (Lord and Eminton)[4], were $C_{D_W} = 0.002_8$ for the 87° model and $C_{D_W} = 0.005_2$ for the 81° model.*

Estimates of zero-lift drag coefficient C_{D_0} constructed from the sum of wave and friction drag estimates have been tabulated as below and compared with the tunnel measurements of C_{D_0}, from which it may be seen that agreement to within about 10% exists.

Table II - 87° Model

Transition	Re	% turbulent	C_{D_F} estimated	C_{D_W} estimated	C_{D_0} estimated	C_{D_0} measured
Free	$2\frac{1}{4} \times 10^6$	33	0.003_8	0.002_8	0.006_6	0.007_5
Free	$5\frac{1}{2} \times 10^6$	50	0.003_8	"	0.006_6	0.007_5
Fixed	$2\frac{1}{4} \times 10^6$	95	0.007_0	"	0.009_8	0.009_0
Fixed	$5\frac{1}{4} \times 10^6$	95	0.005_8	"	0.008_6	0.009_0

*These values are of course for the models with their stings. The corresponding values for models with stings removed, and thus pointed at the rear end, as in flight, are 0.002_6 and 0.006_0, which are not significantly different.

Table III - 81° Model

Transition	Re	% turbulent	C_{D_F} estimated	C_{D_W} estimated	C_{D_0} estimated	C_{D_0} measured
Free	$2\frac{1}{4} \times 10^6$	46	0.003_8	0.005_2	0.009_0	0.008_7
Free	$5\frac{1}{4} \times 10^6$	46	0.003_0	"	0.008_2	0.008_5
Fixed	$2\frac{1}{4} \times 10^6$	73	0.005_0	"	0.010_2	0.009_7
Fixed	$5\frac{1}{4} \times 10^6$	73	0.004_1	"	0.009_3	0.009_5

The wave drags given by an empirical formula due to Collingbourne

$$C_{D_W} = 12 \left(\frac{S_c}{S} \right)^2 \tan \varepsilon$$

where S_c is the maximum cross sectional area, and S is the planform area. are respectively 0.002_0 for the 87° model and 0.004_4 for the 81° model, which are not significantly different from those given by the area rule.

5.22 Drag due to Lift

Since the balance measured axial-force it was considered preferable to use the incremental axial-force with incidence as a direct way of obtaining the drag due to lift and so determine what degree of effective leading edge suction was realised. ΔC_x, the increment in axial-force, and $-C_z \alpha$ are plotted against $-C_z$ for the 81° model in Fig. 6. Thus the ratio of the ordinates of the curves is equivalent to θ/α, where θ is the angle between the resultant force and the normal to the chord. Linear theory gives a value of 0.48 for θ/α for a simple delta planform of 81° leading edge sweepback if full leading-edge suction is developed. From Fig. 6 it appears that the ratio θ/α reaches approximately 0.15 at $-C_z$ of 0.10 at the lower Reynolds numbers.* The theoretical value of 0.48 was not to be expected in view of the fact that the flow separated from the upper surface at quite small incidences, as was shown by flow visualisation tests (see para 5.6), the line of separation moving towards the leading edge with increase of incidence.

In this instance the factor $\frac{K}{K^1}$ used by Courtney[5] to denote the ratio of the observed drag-due-to-lift factor to the drag-due-to-lift factor corresponding to complete loss of leading edge suction would be 0.85.

---

*The value of ΔC_x was beginning to fall off at this normal-force due to the onset of disturbances at the tail of the model caused by sting deflection, which led to a misalignment of the model base and the sting shroud. This drag rise at the lower Reynolds number occurred at the same normal-force, corresponding to a higher normal force coefficient. This has an insignificant effect on L/D ratio however.

On the 87° model, no significant leading edge suction was in fact apparent, from measurements of axial-force increment ΔC_x over the incidence range tested. The precision of measurements was not sufficient to enable any leading edge suction to be detected until an incidence of some 3° was reached but at the C_L for maximum L/D, viz 0.07 ($\alpha = 7\frac{1}{2}^\circ$) it is estimated that the theoretical leading edge suction could have been measured to ±7% accuracy.

5.3 Lift/Drag Ratio

For long range the attainment of a high value of L/D is of the greatest importance, and consequently, in spite of these models not having all the features (such as controls etc) which would characterise real aircraft and their small scale, the tunnel results will be used to give guidance on the long range efficiency of different types of layout. It is probably realistic to regard the drag figures obtained in the tunnel as applicable also in full scale flight since the fully turbulent skin friction at flight Reynolds number will be roughly equal to the partially laminar and partially turbulent skin friction in the tunnel tests at lower Reynolds number.*

Curves of L/D ratios are plotted in Fig. 7. The attainment of full leading edge suction would have given theoretical L/D max. of approximately 7.5 for the 87° model and 8.0 for the 81° model. The values obtained experimentally were 4.2 at C_L of 0.07 and 5.8 at C_L of 0.10 respectively the former being rather low for the long range requirements of this type of aircraft.

5.4 Pitching Moment and Centre of Pressure Position

The reference point about which moments are quoted is $4\frac{1}{2}$" from the nose which is approximately the quarter chord station of the mean aerodynamic chord. The reference length is the mean aerodynamic chord viz, 6.06".

Fig. 8 shows the experimental moment coefficient curve against lift coefficient. In the case of the 81° model an almost straight line passes close to all points and Reynolds number effects and the effects of the transition wire are both very small.

The corresponding curve for the 87° model curves slightly in a direction of decreasing stability, i.e. forward movement of aerodynamic centre, with increasing lift.

Centre of pressure position in terms of centre-line chord length is plotted against incidence in Fig. 9. A slight mean forward movement is apparent for the 81° model, and while it appears that there is a just discernible rearward movement of centre of pressure position due to the higher Reynolds number in the presence of transition wires, no significant change of position occurs without the wires, and a mean line has been drawn through all the points.

In the case of the 87° model the rearward movement of the centre of pressure with Reynolds number is seen to be more pronounced and again the influence of the trip wire is small. The most rearward position of the centre of pressure occurs at an incidence of 3° to 4° and the forward movement with incidence over the range tested is equal to approximately $1\frac{1}{2}$% of the centre-line chord.

---

*The skin friction of the tunnel models with free transition is estimated to be equal to that of an aircraft 120 feet long flying at M = 2.5 at 75,000 ft with a fully turbulent boundary layer.

5.5 Flow Visualisation

Using the evaporating solid technique for boundary layer transition indication, it was found that turbulent flow occurred naturally in the region of maximum thickness of the wing on the 81° model. A wire of 0.006" diameter fixed just back from the leading edge on the upper surface apparently brought the transition forward towards the wire, but the complex nature of the air flow over the surface of a thick delta leaves considerable doubt in the precise interpretation of the indicator pattern.

Oil flow patterns of boundary layer streamlines on both models showed no separations at zero incidence, but the spiral vortex flow arising from flow separations near the leading edge became apparent from very low angles of incidence (refs. 6 and 7).

In Fig. 11, the upper surface oil flow patterns for the 81° model are shown at progressive incidences between 0° and 10°. The sketches of Fig. 10 are included to clarify the photographs which become blurred on shutting down the tunnel. At the lowest incidences it appears that the air flow remains continuous around the leading edge and over the upper surface to a separation line well inboard from the leading edge. "Herring bone" structure suggesting vortex flow appears just inside this separation line towards the rear of the model. With increasing incidence the separation line appears divided; the outer portion moving towards the leading edge, the inner portion denoting the outer boundary of the "herring bone" region maintaining its spanwise position approximately, while the "herring bone" pattern extends forwards. At an incidence of 5° the outer portion of the separation line has almost reached the leading edge and advances little further with incidence. The main vortex pattern tends to increase in intensity, to straighten up minor kinks and to move inboard, so that an extensive "open bubble" region may be supposed to exist behind the leading edge, between it and the vortex, under a vortex sheet. Subsonic flow analogous to this has been reported by Ornberg[8] and by Fink and Taylor[9].

6 Conclusions

The tests were restricted to a comparatively small incidence range by the flexibility of the balance and mounting sting which was designed to measure forces and moments essentially at the incidence of maximum L/D, and emphasis was placed on maintaining the desired body profile uninterrupted by sting mounting as far as possible. This has enabled measurements to be made with greater accuracy at incidences corresponding to cruising conditions appropriate to the role of aircraft under consideration.

The presence of tip fins has complicated any analysis of the lift curve slopes, and until the tests are repeated in the absence of fins it is not possible to estimate their total effect. A preliminary test of the 87° model without fins at M = 2.47 shows that they are responsible for an increment of lift curve slope particularly in the very low incidence range. A corresponding but larger lift curve slope increment with tip fins has been shown to occur at low subsonic speeds with the 87° model.

The measured values of drag at zero lift were predicted with fair agreement by means of a simplified estimate of friction derived from boundary layer transition indicator pictures together with a wave drag estimate by simple area rule.

From curves of the increment of axial force with incidence it has been estimated that some effective leading edge suction component is realised on the 81° model but on the 87° model no significant suction materialised.

The value of the maximum L/D ratio obtained for the 87° model showed the detrimental effect of the extra drag due to the presence of the boundary layer trip ring, but, as has been said, the figures appropriate to the tests without the trip ring is relevant to full scale. The maximum value of L/D for the 87° model was found to be 4.2 occurring at a C_L of 0.07; for the 81° model it was 5.8 occurring at a C_L of 0.10.

Plotted against lift coefficient the pitching moment curves referred to the quarter chord of the mean aerodynamic chord for the 81° model are virtually straight, and the corresponding forward shift of the centre of pressure with incidence is about 10% of the centreline chord over the range tested (α = 0° to 14°). The pitching moment curves for the 87° model show maximum stability at incidences between 3° and 4°. The forward shift of centre of pressure position between 3° and 12° incidence is about 1½% of the centreline chord.

Thus both on the grounds of stability and efficiency as defined by the maximum L/D obtainable the 81° configuration appears to be superior, although by the time allowances have been made for drag due to trim and other practical encumbrances of full scale aircraft the value of L/D available may be diminished.

REFERENCES

No.	Author	Title, etc.
1	Lighthill, M.J.	Supersonic Flow past Bodies of Revolution R. & M. No. 2003. Jan. 1945
2	Küchemann, D.	A non-linear lifting surface theory for wings of small aspect ratios with edge separations. ARC 17769. April 1955
3	Rogers, E.W.E. and Berry, C.J.	Experiments at M = 1.41 on Elliptic Cones with Substantial leading edges. R. & M. 3042. Oct. 1955
4	Lord, W.T. and Brunton, E.	Slender bodies of minimum wave drag giving some area distributions useful in the design of wing body combinations of small theoretical drag rise at transonic speeds. ARC 16786. April 1954
5	Courtney, A.L.	Some effects of flow separation on the overall force characteristics of thin wings of aspect ratio 2 to 4. Unpublished M.O.A. Report. Oct. 1955
6	Weber, J.	Some effects of flow separation on slender delta wings. ARC 18073. Nov. 1955

REFERENCES (Contd)

No.	Author	Title, etc.
7	Maskell, E.C.	Flow separation in three dimensions. ARC 18063 Nov. 1955
8	Ornberg, T.	A note on the flow around delta wings. Swedish K.T.H. F.I. Memo L2. 1953. K.T.H. Aero Tech. Note No. 38. 1954. ARC 16795 (Extract only).
9	Fink, P.T. and Taylor, J.	Some low speed experiments with 20 degree Delta Wings. ARC 17854. Sept. 1955.

WT.2078.C.P.514.53 - Printed in England

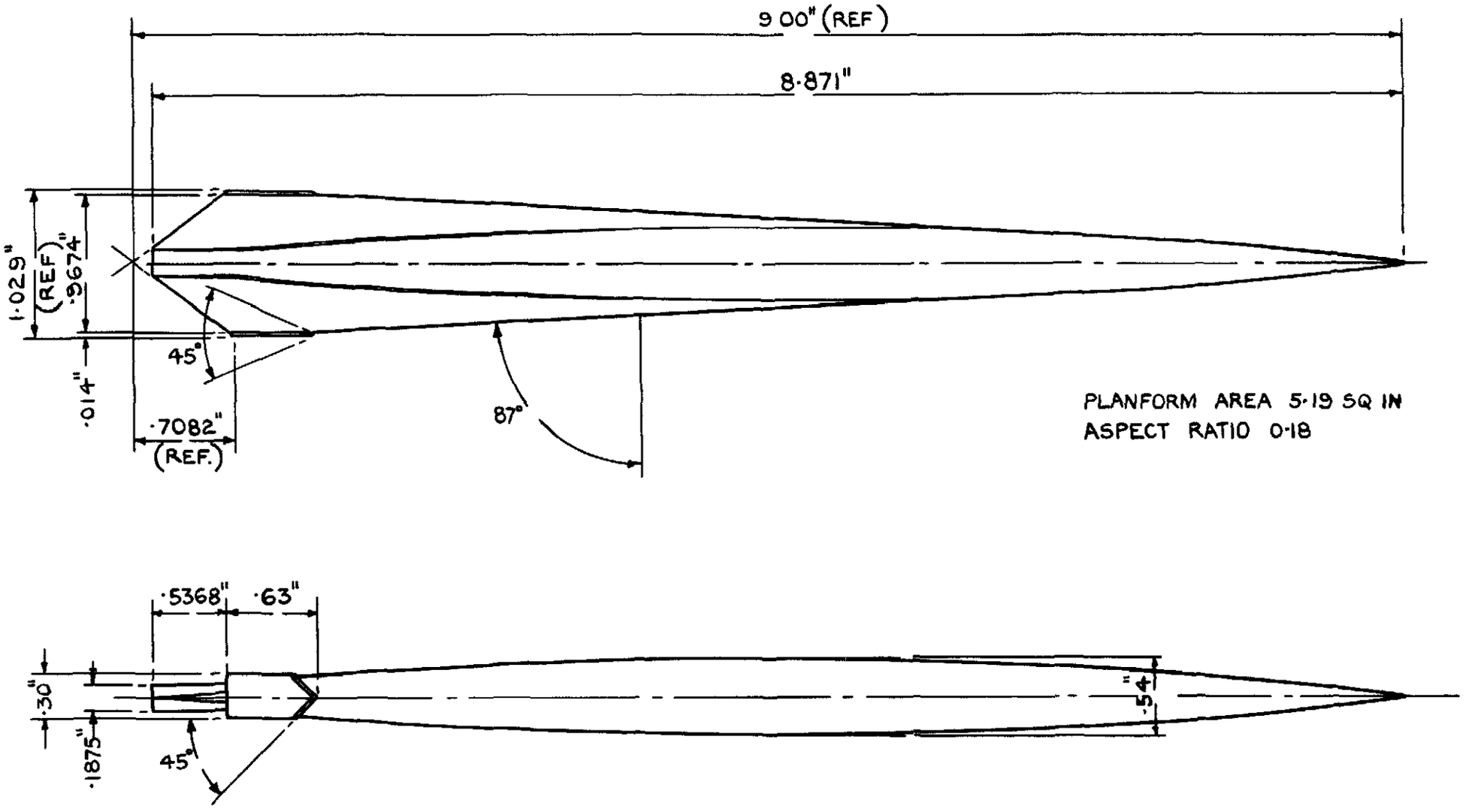

FIG. 1. LEADING DIMENSIONS OF 87° MODEL.

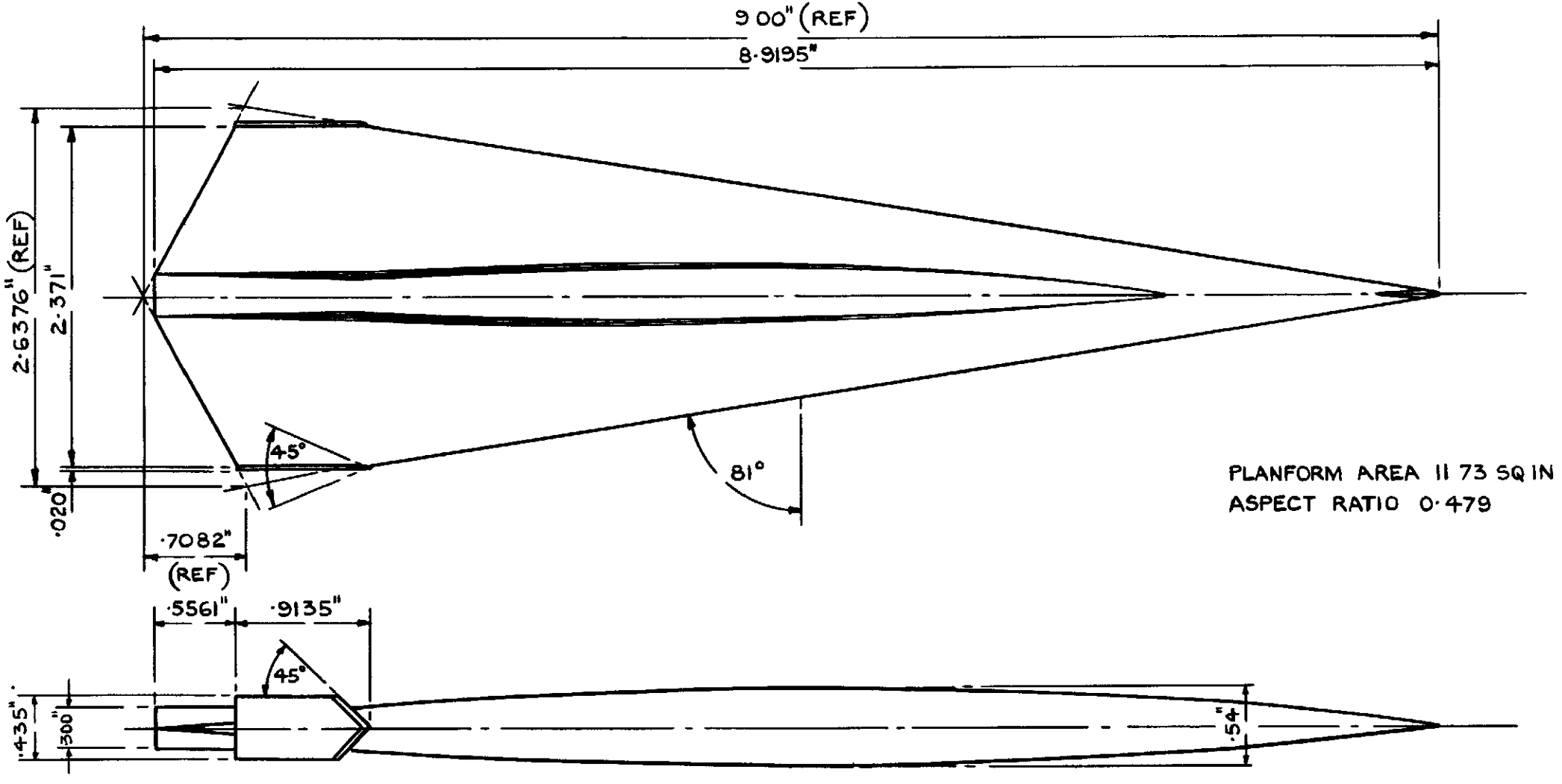

FIG. 2. LEADING DIMENSIONS OF 81° MODEL.

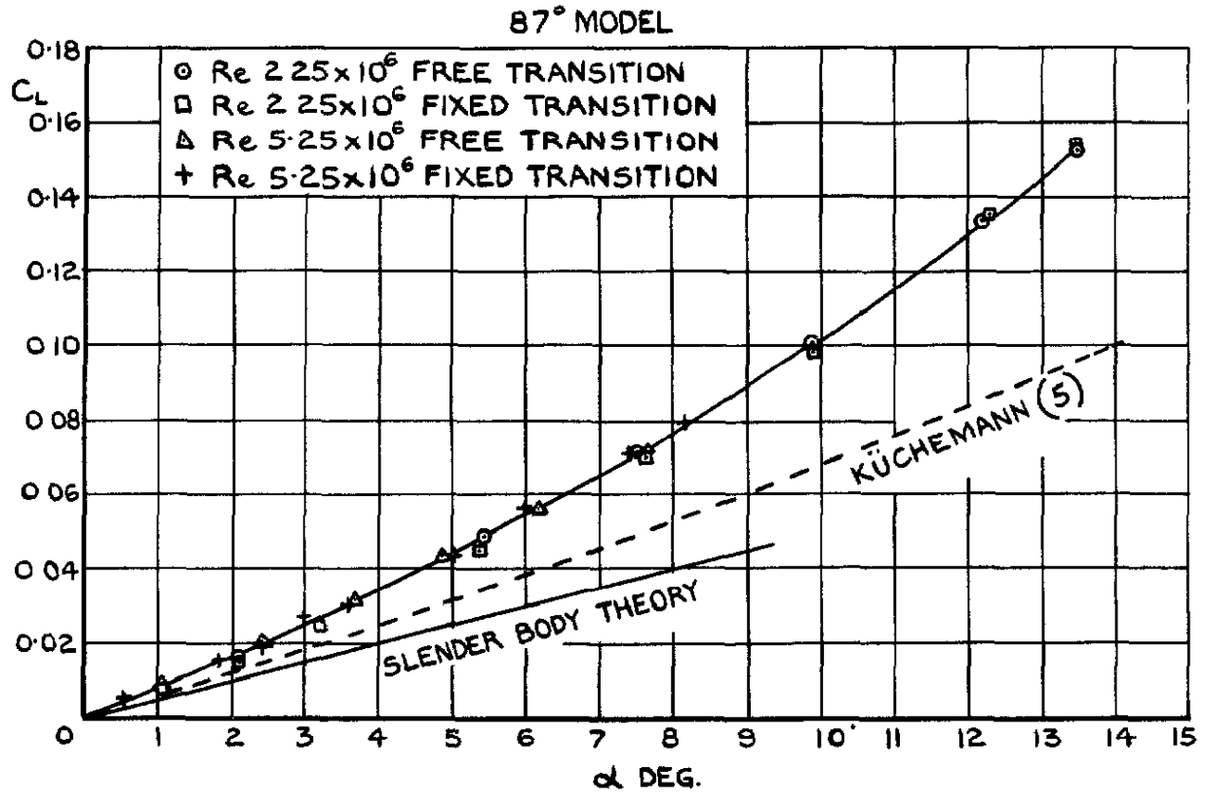

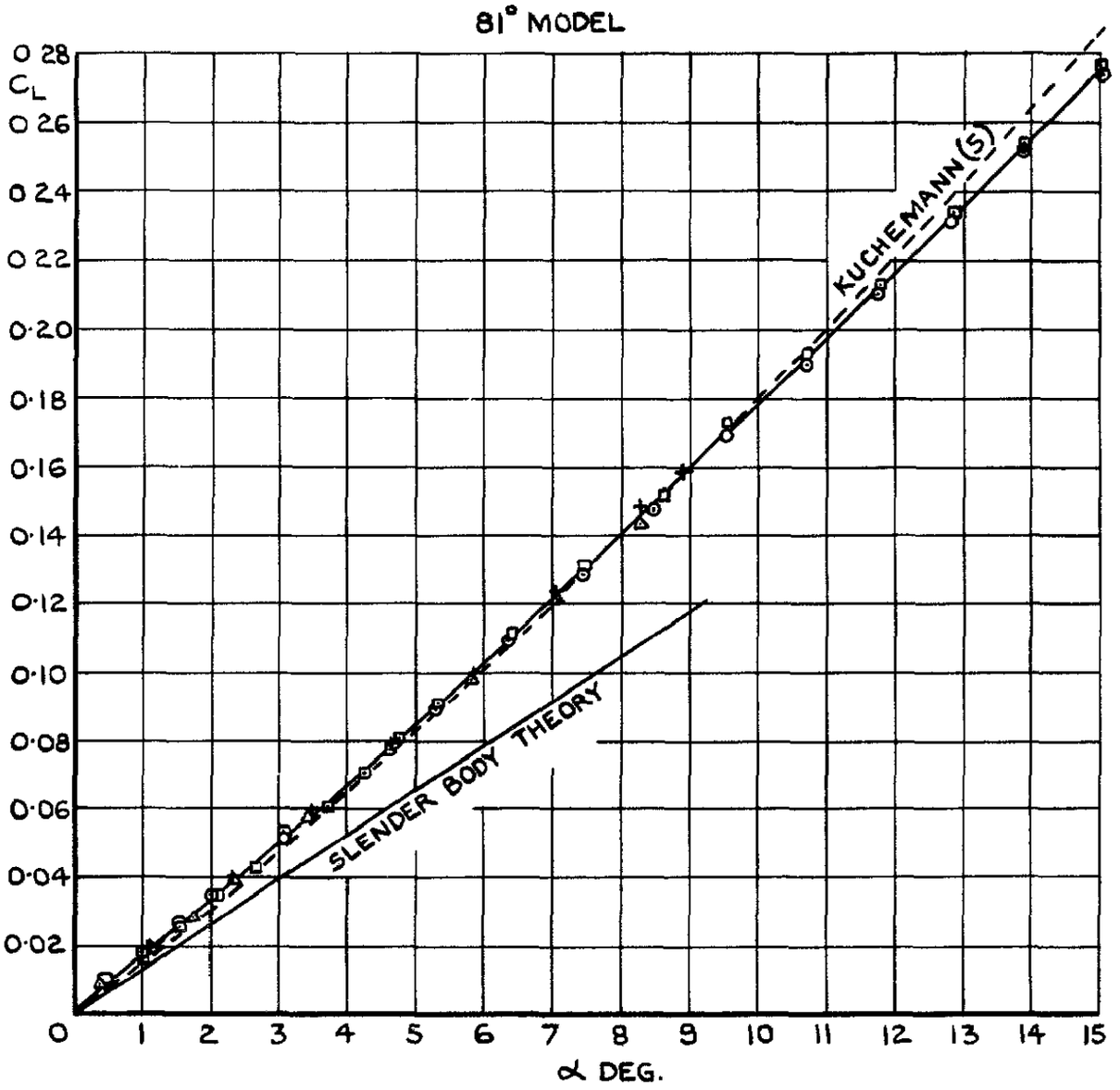

FIG.3. C_L v α° FOR BOTH MODELS AT M = 2·47.

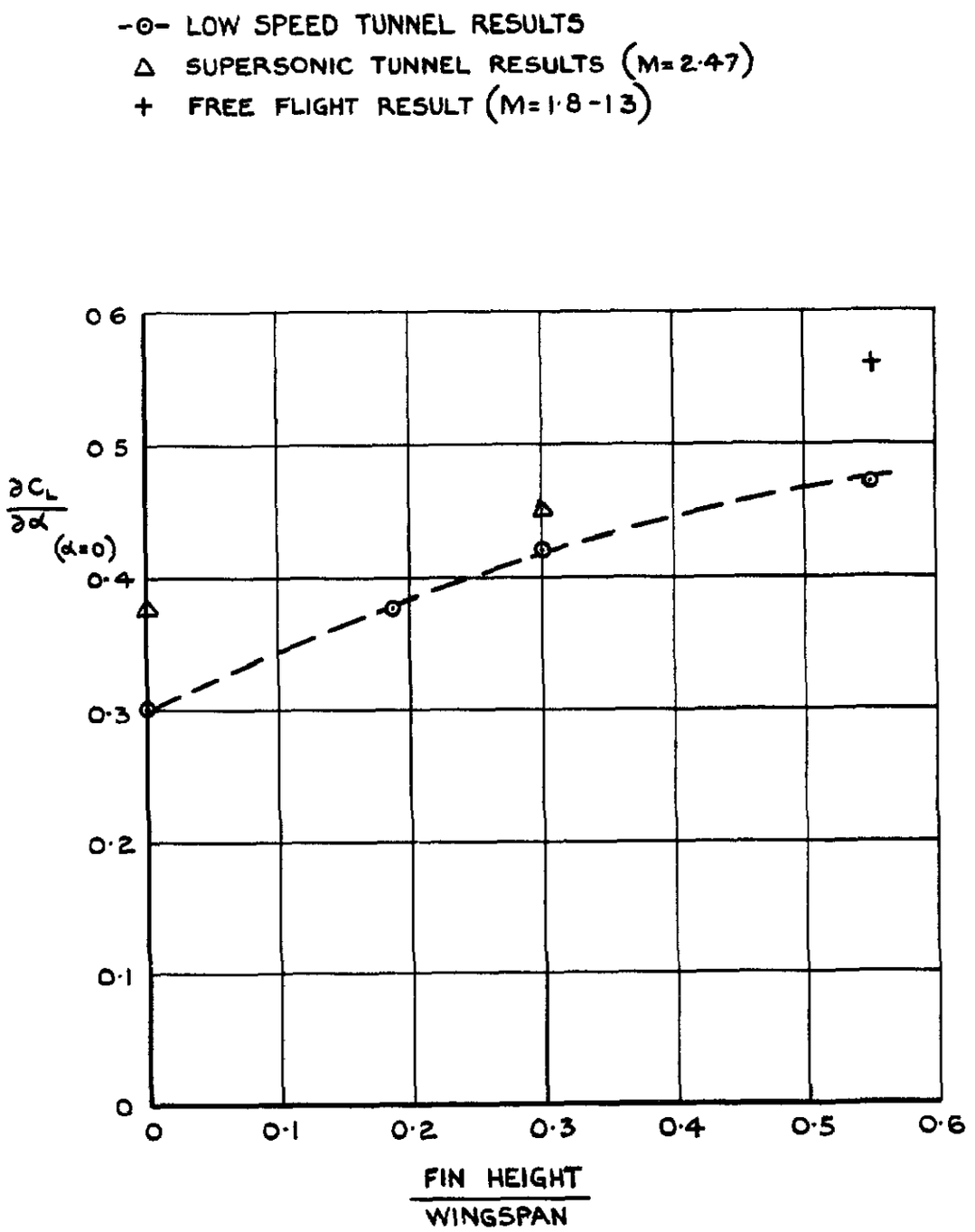

FIG. 4. EFFECT OF TIP FINS ON INITIAL LIFT CURVE SLOPE OF 87° MODEL.

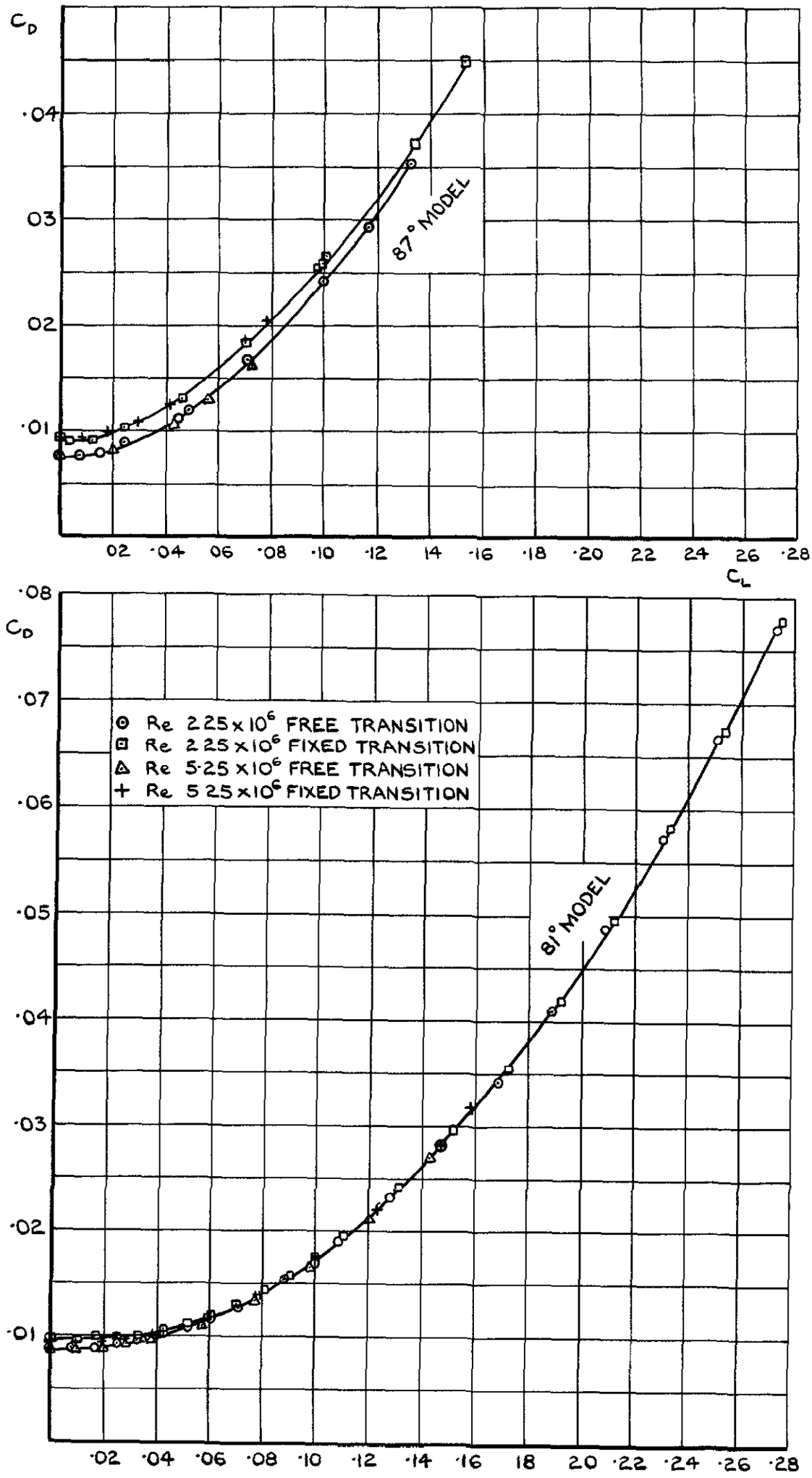

FIG. 5. C_D v C_L FOR BOTH MODELS AT M=2·47.

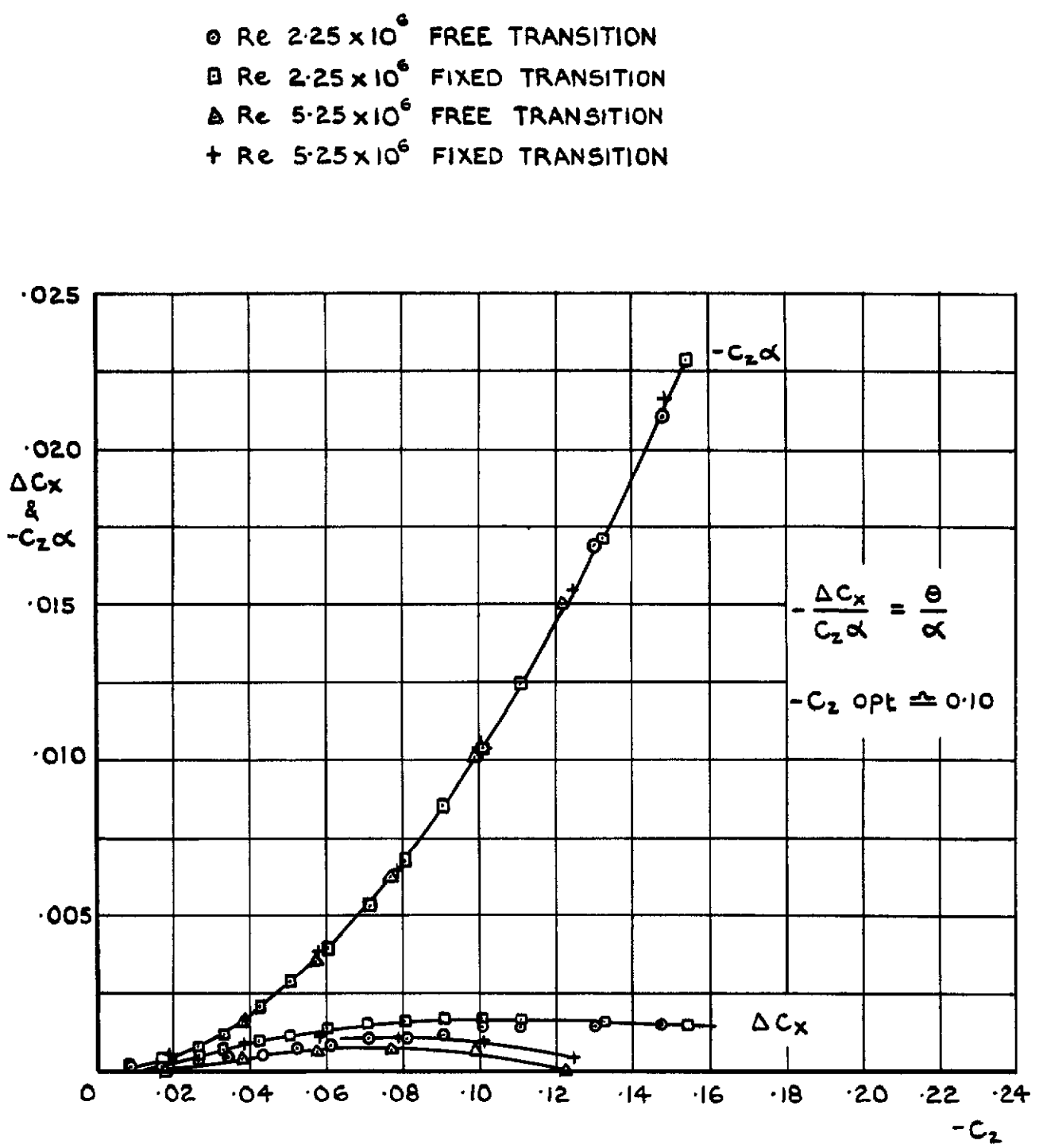

FIG. 6. ΔC_x & $-C_z \alpha$ v $-C_z$ 81° MODEL M = 2·47.

⊙ Re 2·25 x 10^6 FREE TRANSITION
□ Re 2·25 x 10^6 FIXED TRANSITION
Δ Re 5·25 x 10^6 FREE TRANSITION
+ Re 5·25 x 10^6 FIXED TRANSITION

FLAGGED SYMBOLS REFER TO THE 87° MODEL
UNFLAGGED SYMBOLS REFER TO THE 81° MODEL

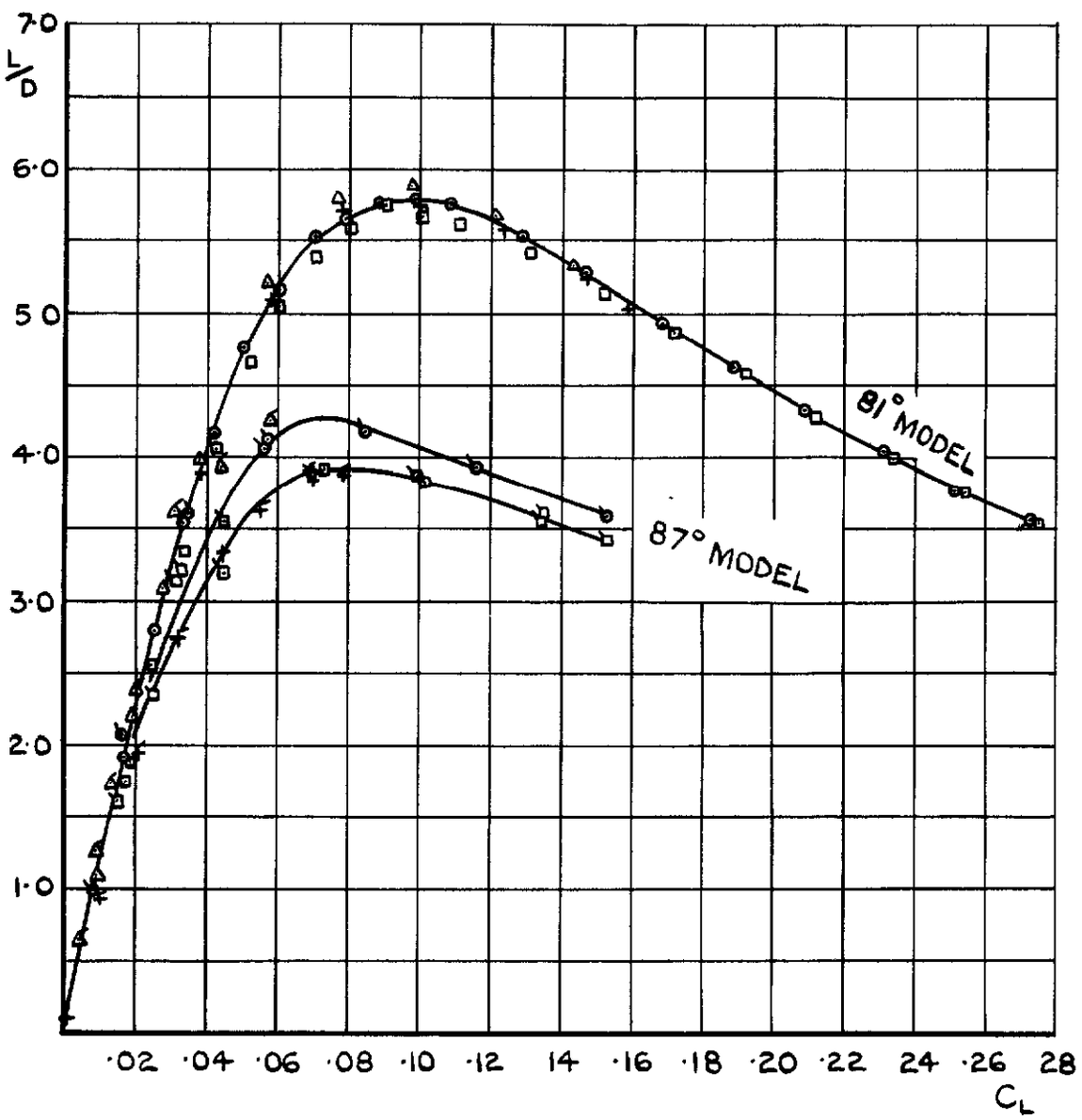

FIG. 7. $\frac{L}{D}$ v C_L FOR BOTH MODELS AT M=2·47.

⊙ Re $2{\cdot}25 \times 10^6$ FREE TRANSITION
⊡ Re $2{\cdot}25 \times 10^6$ FIXED TRANSITION
△ Re $5{\cdot}25 \times 10^6$ FREE TRANSITION
+ Re $5{\cdot}25 \times 10^6$ FIXED TRANSITION

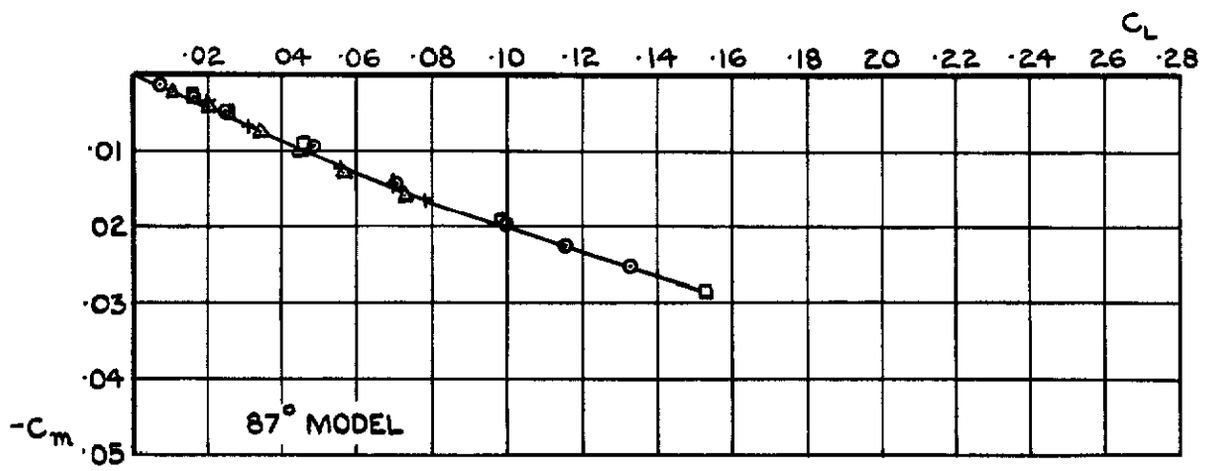

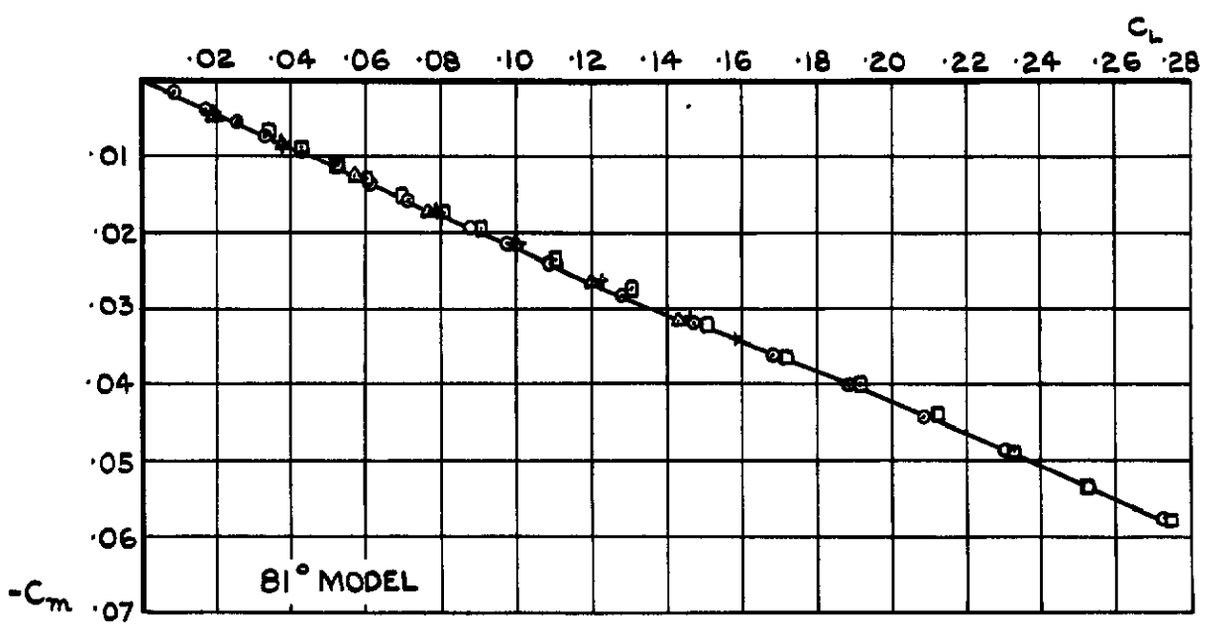

FIG. 8. C_m v C_L FOR BOTH MODELS AT M= 2·47.

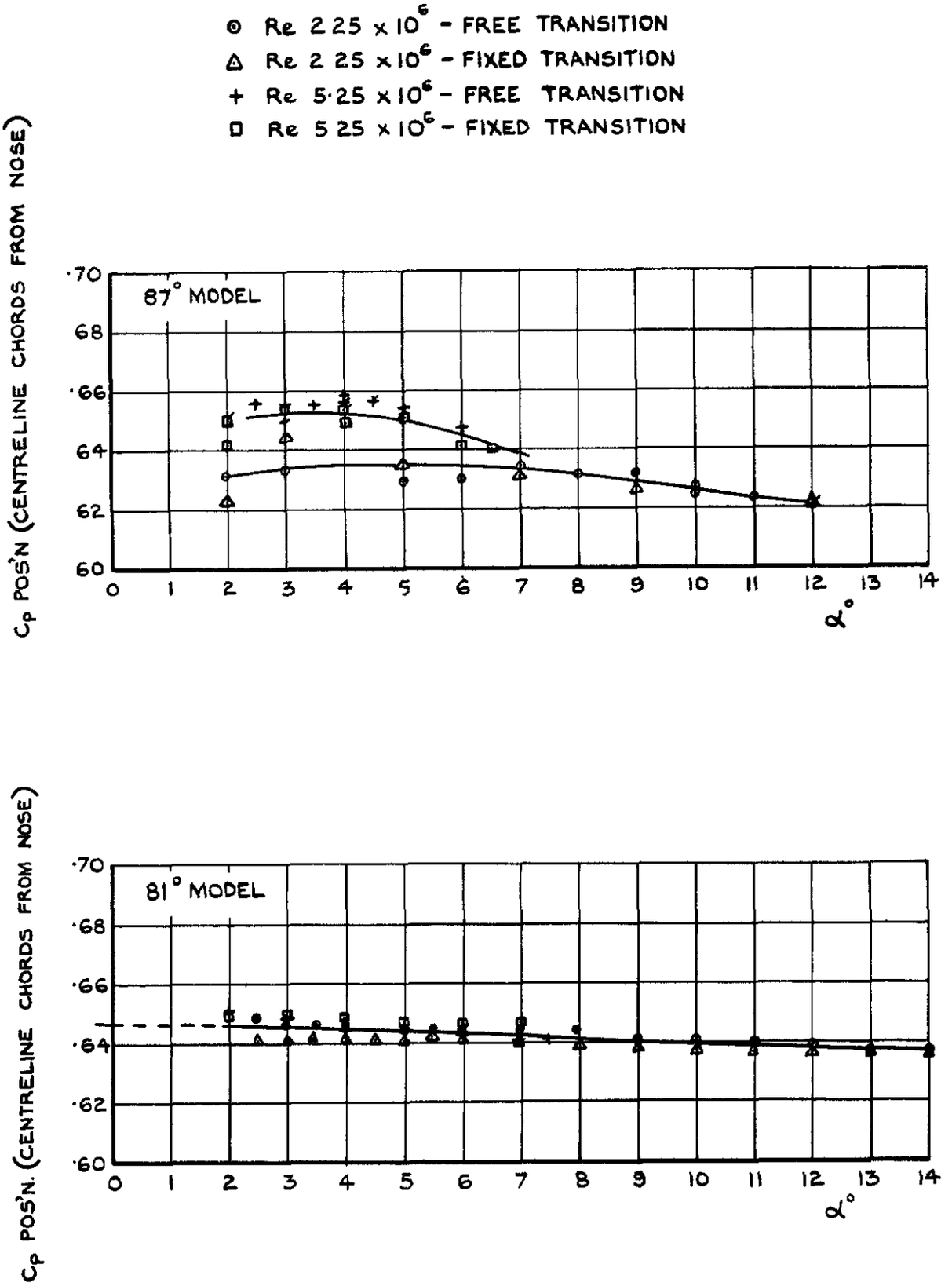

FIG. 9. C_p v α° FOR BOTH MODELS AT M = 2·47.

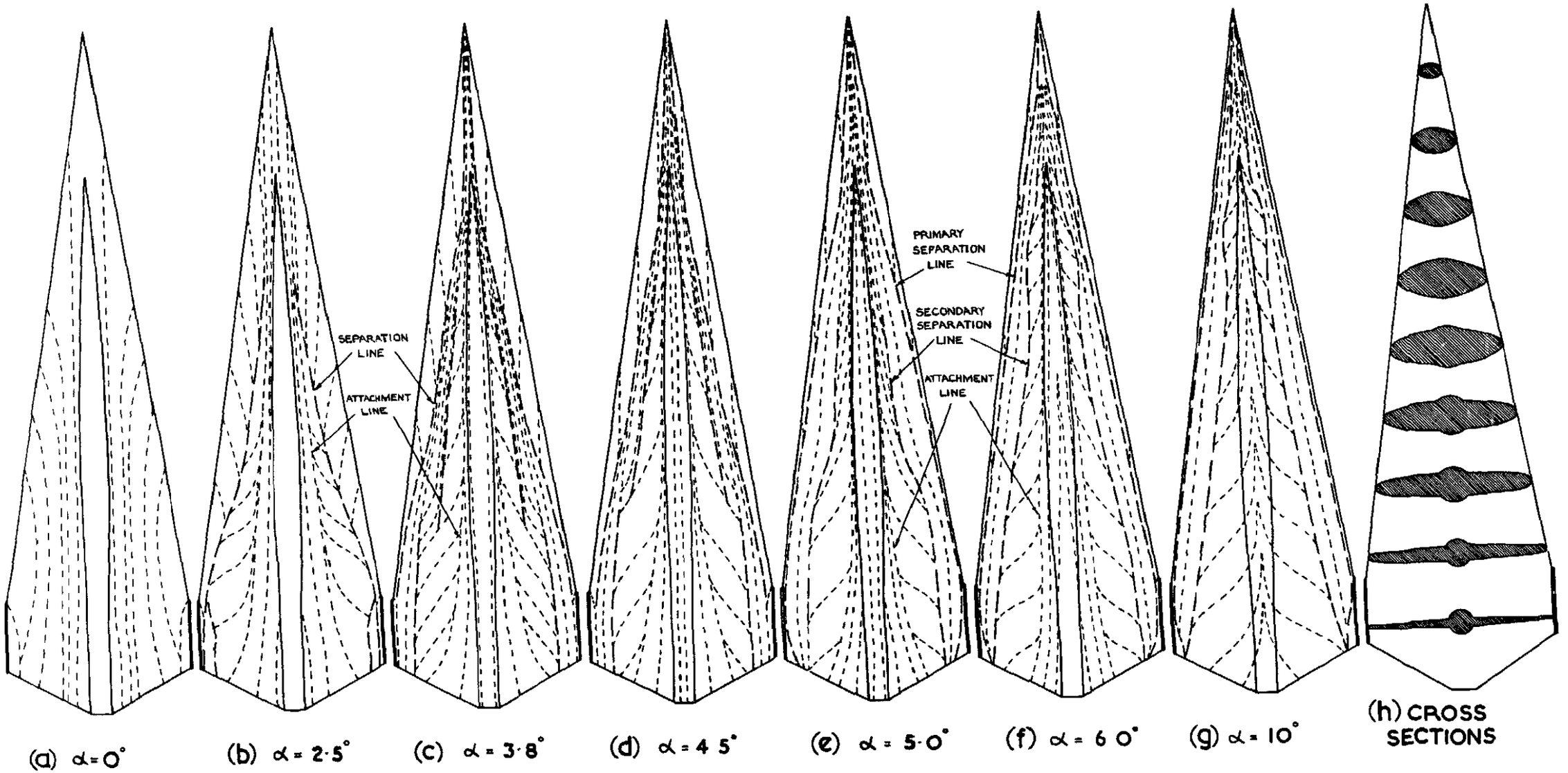

FIG. 10 (a-h). FLOW PATTERNS OVER UPPER SURFACE OF MODEL AT M = 2·47 (DIAGRAMMATIC).

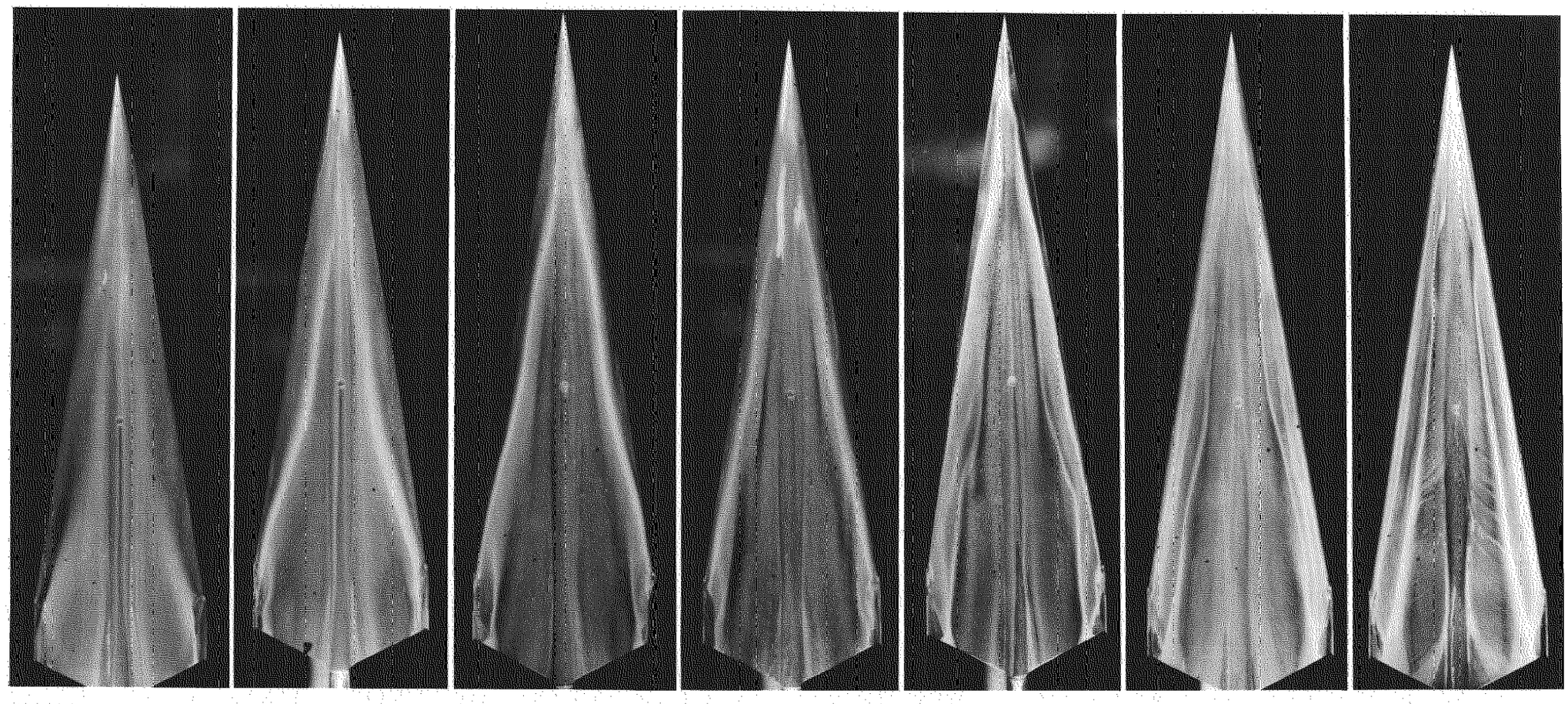

FIG. 11. FLOW PATTERNS OVER UPPER SURFACE OF MODEL 1. AT M = 2.47

C.P. No. 514
(19,868)
A.R.C. Technical Report

Published by
HER MAJESTY'S STATIONERY OFFICE

To be purchased from
York House, Kingsway, London w.c.2
423 Oxford Street, London w.1
13A Castle Street, Edinburgh 2
109 St. Mary Street, Cardiff
39 King Street, Manchester 2
50 Fairfax Street, Bristol 1
2 Edmund Street, Birmingham 3
80 Chichester Street, Belfast 1
or through any bookseller

Printed in England

S.O. Code No. 23-9012-14

C.P. No. 514